Classification of Brain Neuroimaging for Alzheimer's Disease Employing Principal Component Analysis

Fatma S. Shehata, Mostafa Y. Makkey, and Shimaa A. Abdelrahman

***Abstract*—Alzheimer's disease (AD) is one illness that significantly impacts people's lives. As AD worsens over time, it causes the death of brain cells. To assist a neurologist, a proposed classification method for AD progression is introduced in this paper. Pre-processing is applied to clean up artifacts from brain images. As biomarkers for AD diagnosis, three specific areas of the brain are utilized. Multiplicative intrinsic component optimization with an exemplar pyramid is employed for the three main biomarkers segmentation at a multi-scale. For feature extraction, the gray-level co-occurrence matrix is utilized. Finally, principal component analysis is incorporated for feature reduction, and based on the Euclidean distance the decision of the binary classifier is performed. The Alzheimer's Disease Neuroimaging Initiative baseline dataset is used with 311 subjects, 262 for training and 49 for testing. The proposed method achieved an accuracy of 96.296% for the classification between late mild cognitive impairment (LMCI) and cognitive normal (CN), 85.71% between early mild cognitive impairment (EMCI) and CN, 92% between AD and CN, 95.833% between EMCI and LMCI, 91.3% between AD and EMCI, and 84.21% between AD and LMCI. Evaluation results show that the proposed method enhanced the existing method's accuracy with less feature dimensionality.**

***Keywords*—Bias field, Brain segmentation, GLCM, MRI.**

I. INTRODUCTION

Alzheimer's disease (AD) is the sixth leading cause of death worldwide [1]. It affects memory, thinking, and other mental abilities. The exact cause of AD is not fully understood, although many things are thought to increase the risk of developing the disease. These include; age, family history, and untreated depression, although depression can also be a symptom of Alzheimer's lifestyle factors. Signs and symptoms of AD are progressive diseases, which means symptoms develop and eventually get worse over many years. It affects a variety of brain functions. The first sign of AD is usually mild memory problems.

Researchers in [2] specified that certain parts of the brain are among the first to be damaged by AD pathology, whereas other regions only experience impairment in more advanced stages of the disease. These parts can be used as biomarkers for AD. According to [3-4], the white matter (WM) area of AD patients is much lower than that of cognitive normal (CN). Additionally, another study [5] found that reduced hippocampal volume is an early sign of AD pathology measurable by magnetic resonance images (MRI).

In literature [6]-[12], numerous methods have been conducted by analyzing the patient's brain scan for AD diagnosis. The principal component analysis (PCA) method was used to extract distinctive features in [6], and longitudinal and multimodal biomarkers were utilized to diagnose mild cognitive impairment (MCI) patients. Feature extraction techniques including, discrete wavelet transform (DWT), dual-tree complex wavelet transform (DTCWT), and complex wavelet transform (CWT) were employed to extract features from the pre-processed brain MRIs [7].

Gray Level Co-Occurrence Matrix (GLCM) was employed to extract features and then applied the Recursive Feature Elimination (RFE) method to select the most appropriate features [8]. A framework for classifying AD based on texture information extraction was introduced in [9]. The authors utilized three approaches, namely the Fisher score, elastic net regularization, and the support vector machine recursive feature elimination (SVM-RFE) technique to select the best features.

For classification, random forest, linear support vector machine (SVM), and k-nearest neighbor (KNN) algorithms were employed. In [10], Principal Component Analysis (PCA), SPM, GLCM, Local Binary Pattern, deep learning, and Multi-Layer Perceptron were utilized. PCA-based method was introduced in [11], where PCA was developed to extract the features, and partial least squares (PLS) were utilized to leverage the co-variances between various sets of predictors and predicted variables.

PCA with The Independent Component Analysis (ICA) was employed to classify AD and CN [12].

Manuscript received [30 August 2023]; accepted [03 December 2023]. Date of publication [17 January 2024].

Fatma S. Shehata received her BS in Electrical Engineering from Faculty of Engineering, Assuit University, Egypt. Demonstrator at Egyptian German college of technology, Misr International Technology University (MITU), Assuit, Egypt (e-mail: fatmaelzahraa.sayed@itecassiut.edu.eg).

Mostafa Y. Makkey received his BS and MS in Electrical Engineering from Faculty of Engineering, Assuit University, Egypt, and received his Ph.D. in Electrical Engineering from Kent University, UK, with the University of Assiut, (e-mail: mymakkey@ aun.edu.eg).

Shimaa A. Abdelrahman received her B.S. and M.S. degrees in Electrical Engineering from Faculty of Engineering, Assiut University, Egypt. She received Ph.D. degree in Electrical Engineering from Egypt Japan University of Science and Technology (EJUST), Alexandria, Egypt (e-mail: shimaa.adly@aun.edu.eg).

Although many methods were introduced to classify the progression of Alzheimer's disease, there are still some demerits in these methods including; the high dimensionality of the extracted features, requiring massive data sets to train, a large amount of processing time and computational resources to process. Additionally, some of the mentioned methods employed computerized tomography (CT) scans rather than MRI, which include exposure to ionizing radiation, which can increase the risk of cancer compared to MRI scans [13].

In this paper, a proposed method based on the Exemplar pyramid and PCA is introduced to overcome the mentioned limitations in the existing methods. MRI is selected to apply the proposed method, where it has less risk than other imaging techniques. Exemplar pyramid is utilized for subsampling to allow more accurate tracking of disease progression over time. The dimensionality of the extracted features is reduced by employing PCA. Moreover, training on the principal components instead of the original datasets makes the proposed method converge faster than other learning algorithms. The proposed method successfully detects the progression of AD with high accuracy compared to the existing methods.

II. METHODOLOGY

In this paper, a proposed method for the classification of brain scans of the different stages of AD, early mild cognitive impairment (EMCI), late mild cognitive impairment (LMCI), cognitive normal (CN), and AD using the MRI imaging technique is proposed. Six main steps have been introduced including; pre-processing, feature extraction, segmentation, and finally classification as shown in Fig.1.

A. Data collection

For applying the proposed method, the data are obtained from the Alzheimer's Disease Neuroimaging Initiative (ADNI) database [14], namely MPRAGE. In total, 311 structural T1-weighted MRI scans with thicknesses of 1.2mm are used from a 3 Tesla Philips Medical System, flip angle of 9°, and (256, 256,170) matrix. Male and female elderly people between the ages of 75 and 95 are selected for this experiment. The utilized dataset consists of 106 CN images, 84 EMCI, 65 LMCI, and 56 AD.

B. Preprocessing and Segmentation

The first step in the proposed method is image preprocessing, where intensity inhomogeneity and inherent artifact that causes gradual intensity fluctuations in the same tissue present a difficulty in the segmentation step [15]. The static (B0) and transmitted (B1) field in-homogeneities and patient-specific interactions are causes of intensity inhomogeneity in MRI. The ranges of intensities of several tissues overlap as a result of intensity heterogeneity, which frequently results in incorrect tissue classification. Therefore, before doing a quantitative analysis of the MRI scans, it is frequently a requirement to remove the intensity inhomogeneity using a bias field correction. In the last two decades, a large number of bias field correction techniques have been presented [16-18].

The multiplicative intrinsic component optimization (MICO) method [15] is employed in this paper to perform a bias field correction and segment the three main biomarkers of the brain based on the energy minimization formulation concept. To apply the MICO method, the following steps are applied:

1) **MR image I is modeled as in (1) [15]**.

$$I_{(x)} = b_{(x)} J_{(x)} + n_{(x)} \quad (1)$$

Where $I_{(x)}$ stands for the uncorrected bias field image's intensity at pixel x, $J_{(x)}$ for the corrected bias field image's intensity at pixel x, $b_{(x)}$ for the bias field, and $n_{(x)}$ for additive noise with zero means.

2) **Bias field $b_{(x)}$ is expressed as in (2)[15]**.

$$b_{(x)} = W^T G_{(x)} \quad (2)$$

Where $W = (w_1, w_2, \cdots, w_M)^T$ stands for the column vector of observed optimal coefficients $w_1, w_2, \ldots, w_M$, $G_{(x)} = (g_{1(x)}, g_{2(x)}, \ldots, g_{M(x)})^T$ stands for the smooth column vector-valued function of basis functions $g_{1(x)}, g_{2(x)}, \ldots, g_{M(x)}$, and M for a number of coefficients. Image's domain has three types of tissues (WM, GM, and CSF), for pixel x in the L^{th} tissue. The corrected image $J_{(x)}$ is approximately equal to a constant C_L, and the membership function u_L of each L^{th} region (tissue).
The corrected bias field image $J_{(x)}$ is expressed as in (3) [15].

$$J_{(x)} = \sum_{L=1}^{3} C_L u_{L(x)} \quad (3)$$

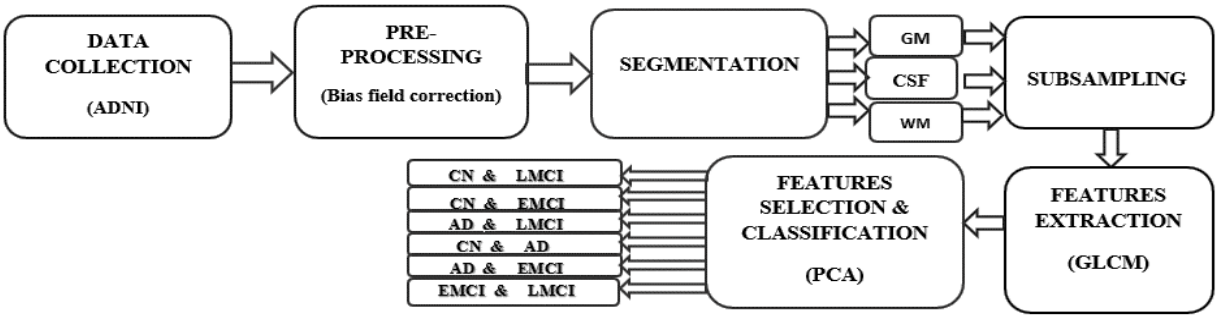

Fig.1. Steps for classification of MR brain images for AD

Finally, the optimization of $b_{(x)}$ and $J_{(x)}$ can be achieved by minimizing the energy function concerning u, C, and W by using energy function equations in [15].

As a result of minimizing the energy function the optimal membership function u is the segmentation result.

C. *Subsampling*

The subsampling process plays an important role in the classification of Alzheimer's disease by reducing noise, increasing computing efficiency (enabling faster processing and analysis), and improving the classification between different brain patterns [19].

For subsampling, the exemplar pyramid method comes in a variety of types, including low passes and band passes. This approach allows for more accurate tracking of disease progression over time. According to a study [10], for classifying Alzheimer's disease stages, the exemplar pyramid is a reliable and valid method for subsampling.

D. Features Extraction

GLCM [20] is one of the most popular methods for extracting texture features in the study of medical images. It represents the distribution of converging color or grayscale value of pixels at a specific offset to analyze the texture of the images. In the proposed method, GLCM method is employed to texture-related features that have high discriminatory power, such as contrast, correlation, homogeneity, and entropy.

1) **Contrast:**

It calculates the local variations in the GLCM, where it measures the intensity transition between two pixels as in (4) [10].

$$\text{Contrast}=\sum_{i,j=0}^{N-1}(i-j)^2\ P(i,j) \tag{4}$$

Where N is the number of rows and columns of the GLCM, P(i,j) is the value of the element in the GLCM at the i^{th} row and j^{th} column.

2) **Correlation:**

It calculates the joint probability occurrence between two pixels as in (5) [10].

$$\text{Correlation}=\sum_{i,j=0}^{N-1}\left(\frac{(i-\mu_i)(j-\mu_j)}{\sigma_i\sigma_j}\ P(i,j)\right) \tag{5}$$

Where μi and μj are the mean of the i^{th} row and j^{th} column of the GLCM respectively, σi and σj are the standard deviations of the i^{th} row and j^{th} column of the GLCM respectively.

3) **Homogeneity:**

It measures the closeness of the elements in a GLCM matrix to its diagonal as in (6) [10].

$$\text{Homogeneity}=\sum_{i,j=0}^{N-1}\frac{P(i,j)}{(1+|i-j|)} \tag{6}$$

4) **Entropy:**

It measures any disorder in an image, more non-uniformity texture is obtained with entropy larger value, the Entropy of that image [10-21] as in (7) [10].

$$Entropy=\sum_{i,j=0}^{N-1}-\ln\left(P(i,j)\right)P(i,j) \tag{7}$$

E. Features Reduction and Classification

Reduction of the feature dimensionality is a process of retaining the most important information from the raw data with less dimensionality. In the proposed method, PCA [22] is employed for this purpose. This process involves transforming the raw data into a set of features that can be easily analyzed and interpreted to prepare data for further processing as classification as shown in Fig. 2.

The training feature vectors are normalized to make all features at the same scale and to eliminate the influence of different dimensions. This is performed by subtracting the mean of each feature vector and dividing it by its standard deviation to obtain a normalized dataset. Then the covariance matrix of the normalized dataset is computed. Eigenvectors (represent the principal components) and eigenvalues (represent the variance of each principal component) of the covariance matrix are calculated. In descending order, the eigenvectors are sorted based on their corresponding eigenvalues to make sure that the principle components are ordered according to the amount of variance they explain.

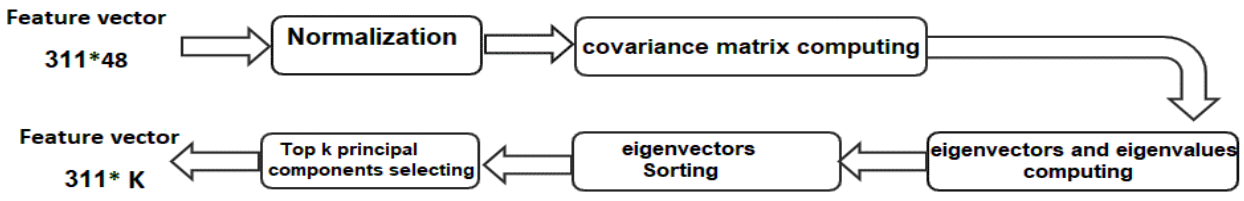

Fig.2. Steps for the PCA algorithm

Finally, the top k principal components (The top k eigenvectors correspond to the k largest eigenvalues) are selected. The following equations indicate the steps to apply the PCA.

1) **Normalized the feature matrix, as expressed in (8)[23]**

$$D(y,h)_{norm} = \frac{D(y,h) - \mu}{\sigma} \quad (8)$$

Where $D(y,h)_{norm}$ is the normalized feature matrix , y is the number of images, h is the number of observations in the features matrix., and D(y,h) is the feature matrix of the MRI images , μ is the mean vector of the feature vectors, and σ is the standard deviation vector of the feature vectors.

2) **Compute the covariance matrix, as expressed in (9) [24]**

$$A = \frac{1}{h} D(y,h)_{norm}{}^{T} D(y,h)_{norm} \quad (9)$$

Where A is the covariance matrix of the normalized feature vector with dimensions of h x h.

3) **Compute the eigenvectors and eigenvalues that achieved as expressed in (10) [24].**

$$AZ = \lambda Z \quad (10)$$

Where λ is an eigenvalue of the A matrix associated with eigenvector Z of a covariance matrix.

4) **Select the top k principal components that correspond to the k largest eigenvalues.**

5) **Project the standardized feature vectors onto the top k.**

F. Classification

For the classification of Alzheimer's disease progression, Euclidean distance is calculated between two vectors, testing, and each training feature vector, using (11) [25].

$$d_j(x_i, y_j) = \sqrt{\sum_{i=1}^{B} (x_i - y_j)^2} \quad J=1,2,.....F \quad (11)$$

Where $d_j(x_i, y_j)$ is the Euclidean distance for j^{th} testing image between i^{th} training feature vector x_i and j^{th} testing feature vector y_j B and F are the total number of training and testing feature vectors respectively. Based on the minimum distance, the output of the classifier will be one of two decisions, LMCI or CN, EMCI or CN, AD or CN, EMCI or LMCI, AD or EMCI, and AD or LMCI.

III. Results And Discussion

The proposed method was implemented on MATLAB R2018a using 80 and 20% for training and testing respectively. As a preprocessing step, we used an iterative technique to minimize the energy and estimate the bias field. MRI image and its corresponding corrected bias field image are shown in Fig. 3. In the segmentation step, the preprocessed images are segmented by the MICO method into GM, WM, and CSF as shown in Fig. 4.

In the subsampling step, the low pass exemplar pyramid method is applied. Bi-linear interpolation is employed for this purpose, where the segmented MRI images are subsampled in the vertical and horizontal coordinate directions by a factor of 2. The resultant images are shown in Fig. 5. To find characteristics of an image that are rotationally invariant, the sum of the co-occurrence matrices at several regular angles (for example, 0, 45, 90, and 135 degrees) is used to accurately classify patients into different stages of the disease. For feature reduction, considering that an image's energy is focused in its first few component vectors, the top eight principal components give the direction of the largest variance of features. The magnitude of eigenvalue is plotted in decreasing order as shown in Fig. 6. Distance is calculated to determine the class to which an unknown feature vector belongs. For classification evaluation, a comparison with existing methods is summarized in Table I.

The proposed method achieves the highest accuracy of 96.296% for the binary classification between LMCI and CN, 85.71% between EMCI and CN, 92% between AD and CN, 95.833% between EMCI and LMCI, 91.3% between AD and EMCI, and 84.21% between AD and LMCI.

It is observed that, the highest accuracy of the proposed method is occurred as a result of more than one enhancement method compared with the existing methods. Bias field correction is used to remove the intensity inhomogeneity. Employing different scales in order to study all the relevant features and improve the classification between different brain patterns. Moreover, PCA is employed which facilitates feature reduction, reduces the computing burden, and simplifies the analysis. Combination of GM, WM, and CSF; CSF, and GM; CSF and WM; GM and WM; CSF, GM, and WM are studied to achieve the highest accuracy as illustrated in Table II. From this table, it can be observed that combination of GM and CSF gives the highest accuracy in most cases, comparisons between the accuracies in each case are indicated in this table.

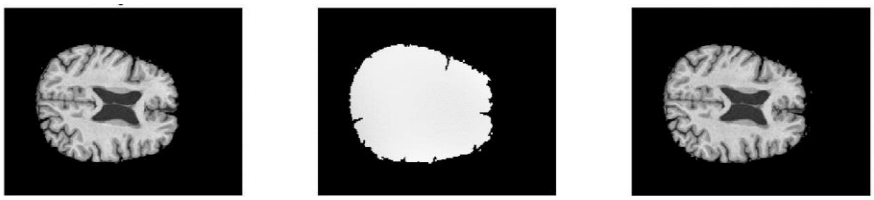

(a) (b) (c)

Fig.3. (a) Original image, (b) Estimated bias field, and (c) Bias field corrected image.

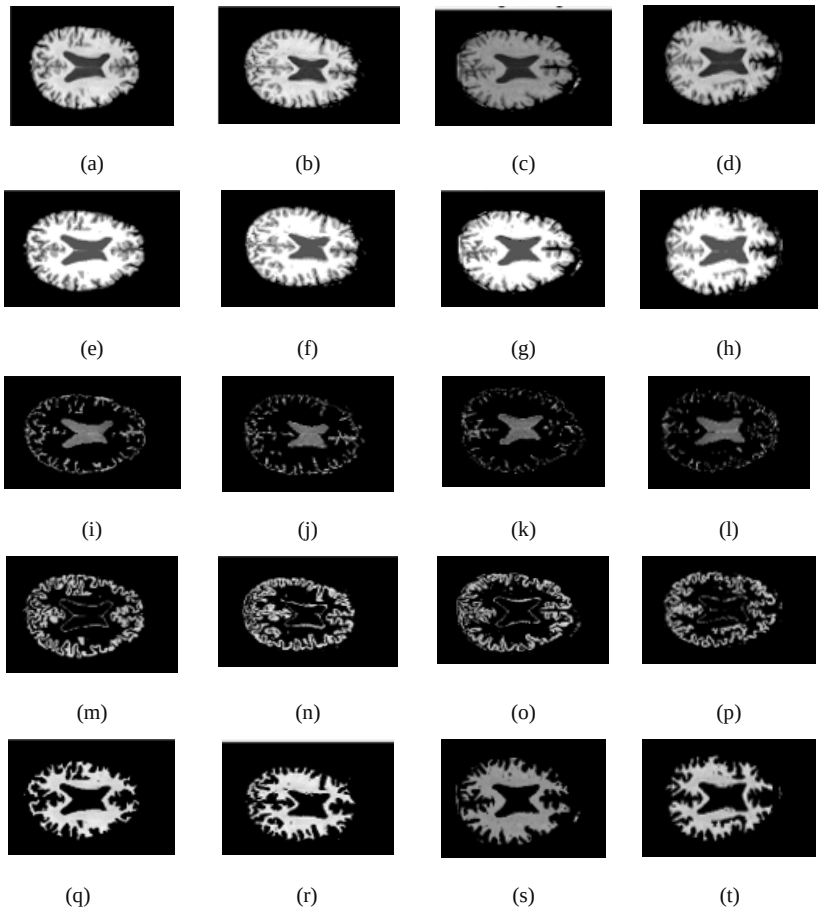

(a) (b) (c) (d)

(e) (f) (g) (h)

(i) (j) (k) (l)

(m) (n) (o) (p)

(q) (r) (s) (t)

Fig.4. The original MRI image of (a) AD, (b) CN (c) EMCI, and (d) LMCI, Segmentation result of (e) AD, (f) CN (g) EMCI, and (h) LMCI, and The corresponding resultant segmented image (i) CSF of AD, (j) CSF of CN (k) CSF of EMCI, and (l) CSF of LMCI, (m) GM of AD, (n) GM of CN (o) GM of EMCI, and (p) GM of LMCI, (q) WM of AD, (r) WM of CN (s) WM of EMCI, and (t) WM of LMCI

TABLE I

COMPARISON BETWEEN PROPOSED AND EXISTING CLASSIFICATION METHOD

Method	Year	Classifier Classes	Accuracy	Total Sample	Training Samples	Total Training Samples	Testing Samples	Total Testing Samples
V. Krishna Kumar, et al. [9]	2019	AD vs CN	87.39%	812 (CN =227, AD=189, MCI = 396)	AD = 93, CN = 93	186	AD = 96, CN = 134	230
		AD vs MCI	63.16%		AD =93, MCI =93	186	AD =96, MCI =303	399
		CN vs MCI	64,74%		CN =113, MCI =113	226	CN =114, MCI =283	397
Zaina , H.S, et al. [10]	2022	CN vs EMCI	96.43%	311 (CN =106, AD = 57, EMCI = 83, LMCI =65)	CN+EMCI = 161	161	CN+EMCI = 28	28
		EMCI vs AD	90.91%		EMCI+AD= 118	118	EMCI+AD= 22	22
		LMCI vs AD	95.24%		LMCI+ AD =101	101	LMCI+ AD =21	21
		EMCI vs LMCI	95.65%		EMCI+LMCI =125	125	EMCI+LMCI =23	23
		CN vs LMCI	100%		CN+LMCI= 144	144	CN+LMCI= 27	27
		CN vs AD	96.15%		CN+AD =137	137	CN+AD =26	26
L.Khedher, et.al [11]	2015	AD vs CN	88.49%	818 (CN=229, MCI=401, AD=188)	CN+MCI+AD=737	737	CN+MCI+ AD=81	81
		MCI vs AD	87.03%	555 (CN=185, MCI=185, AD=185)	MCI+AD =333	333	MCI+AD =37	37
		MCI vs CN	81.89%		MCI+CN =333	333	MCI + CN =37	37
I. Illán, et. Al [12]	2011	AD vs CN	88.24%	401 (CN= 97, MCI=209, AD=95)	AD=53, CN=52	105	AD=42, CN=45	87
		MCI vs CN	70.21%		MCI=114, CN= 52	166	MCI=95, CN= 45	140
Proposed Method	2023	LMCI vs CN	96.296%	311 (CN =106, AD = 56, EMCI = 84, LMCI =65)	LMCI =54, CN =90	144	LMCI =11, CN =16	27
		EMCI vs LMCI	95.833%		EMCI =70, LMCI =54	124	EMCI =14, LMCI =11	25
		AD vs CN	92 %		AD =47, CN =90	137	AD =9, CN =16	25
		AD vs EMCI	91.3%		AD =47, EMCI =70	117	AD =9, EMCI =14	23
		EMCI vs CN	85.71%		EMCI =70, CN =90	160	EMCI =14, CN =16	30
		AD vs LMCI	84.21%		AD =47, LMCI =54	101	AD =9, LMCI =11	20

TABLE II

COMPARISON BETWEEN ACCURACIES

Classification	Feature Matrix	Accuracy %
LMCI &CN	CSF	85.18%
	GM	81.48 %
	WM	70.37 %
	[CSF GM]	**96.29 %**
	[CSF WM]	77.77 %
	[GM WM]	74.07 %
	[CSF GM WM]	81.48 %
EMCI& LMCI	CSF	70.80%
	GM	79.17%
	WM	79.17%
	[CSF GM]	**95.83%**
	[CSF WM]	79.17%
	[GM WM]	66.66%
	[CSF GM WM]	79.17%
AD &CN	CSF	76.00%
	GM	68.00%
	WM	68.00%
	[CSF GM]	80.00%
	[CSF WM]	**92.00%**
	[GM WM]	84.00%
	[CSF GM WM]	**92.00%**
AD & EMCI	CSF	82.60%
	GM	**91.30%**
	WM	78.26%
	[CSF GM]	**91.30%**
	[CSF WM]	82.60%
	[GM WM]	**91.30%**
	[CSF GM WM]	**91.30%**
EMCI &CN	CSF	81.48%
	GM	81.48%
	WM	81.48%
	[CSF GM]	78.57%
	[CSF WM]	75.00%
	[GM WM]	**85.71%**
	[CSF GM WM]	78.57%
AD & LMCI	CSF	63.15%
	GM	73.68%
	WM	63.15%
	[CSF GM]	**84.21%**
	[CSF WM]	73.68%
	[GM WM]	73.68%
	[CSF GM WM]	**84.21%**

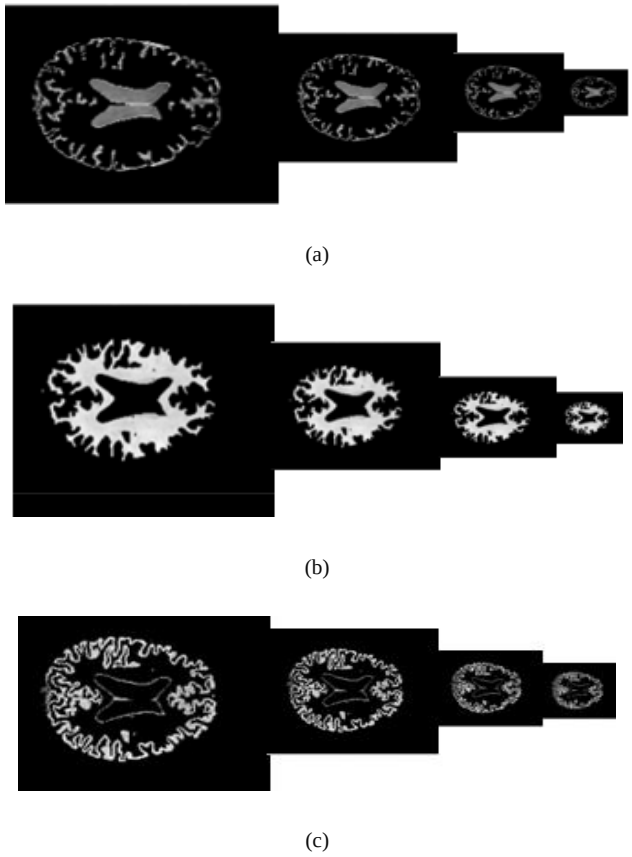

(a)

(b)

(c)

Fig. 5. The implementation of the exemplar pyramid on (a) CSF, (b) GM, and (c) WM segmented images.

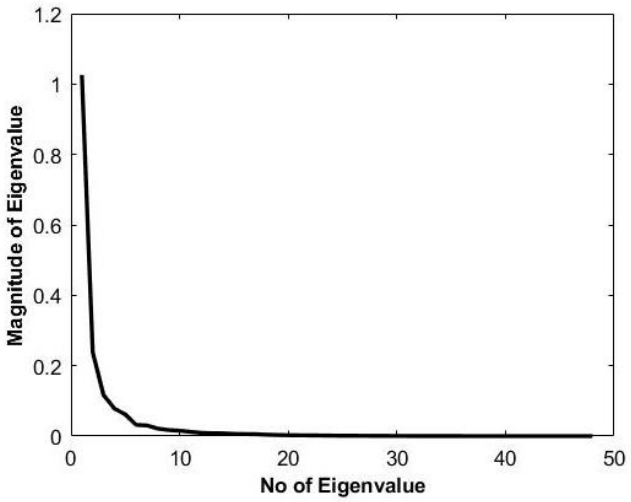

Fig. 6. The magnitude of the eigenvalues in decreasing order

IV. CONCLUSION

In this paper, a proposed method to classify Alzheimer's disease stages is proposed. Datasets (CN, EMCI, LMCI, and AD image) downloaded from ADNI are employed and divided into training and testing. The MICO method was used for bias field estimation and segmentation of MRI images into GM, WM, and CSF. The resultant segmentation images are downscaled three times for more accurate and consistent classification results. GLCM was used to extract features, and finally, for classification, PCA and the minimum Euclidian distance were employed. Different combination of the extracted features for each brain biomarker is studied. The final results show that the proposed method has successfully classified MRI images with the highest accuracy of 96.296 %compared with existing methods.

REFERENCES

[1] R. U. Haque and A. I. Levey, "Alzheimer's disease: A clinical perspective and future nonhuman primate research opportunities," Proc. Natl. Acad. Sci. U. S. A., vol. 116, no. 52, pp. 26224–26229, 2019.

[2] G. Uysal and M. Ozturk, "Hippocampal atrophy-based Alzheimer's disease diagnosis via machine learning methods," Journal of Neuroscience Methods, vol. 337, 2020.

[3] M. L. F. Balthazar, C. L. Yasuda, F. R. Pereira, T. Pedro, B. P. Damasceno, and F. Cendes, "Differences in grey and white matter atrophy in amnestic mild cognitive impairment and mild Alzheimer's disease," Eur. J. Neurol., vol. 16, no. 4, pp. 468–474, 2009.

[4] L. Frings et al., "Longitudinal grey and white matter changes in frontotemporal dementia and Alzheimer's disease," PloS one, vol. 9, no. 3, 2014.

[5] A. T. Du et al., "Magnetic resonance imaging of the entorhinal cortex and hippocampus in mild cognitive impairment and Alzheimer's disease," J. Neurol. Neurosurg. Psychiatry, vol. 71, no. 4, pp. 441–447, 2001.

[6] D. Zhang and D. Shen, "Predicting future clinical changes of MCI patients using longitudinal and multimodal biomarkers," PloS one, vol. 7, no. 3, 2012.

[7] U. R. Acharya, S. L. Fernandes, J. E. Weikoh, and E. J. Ciaccio, "Automated detection of Alzheimer's disease using brain MRI images- A study with various feature extraction techniques,'','' J. Med. Syst, vol. 43, 2019.

[8] Z. Xiao, Y. Ding, T. Lan, and C. Zhang, "Brain MR image classification for Alzheimer's disease diagnosis based on multi-feature fusion," Comput. Math. Methods Med, vol. 2017, pp. 1–13, 2017

[9] K. Vaithinathan and L. Parthiban, "Alzheimer's disease Neuroimaging Initiative, "A novel texture extraction technique with T1 weighted MRI for the classification of Alzheimer's disease," J. Neurosci. Methods, vol. 318, pp. 84–99, 2019.

[10] H. S. Zaina, S. B. Belhaouari, T. Stanko, and V. Gorovoy, "An exemplar pyramid feature extraction based Alzheimer disease classification method," IEEE Access, vol. 10, pp. 66511–66521, 2022.

[11] L. Khedher, J. Ramírez, J. M. Górriz, A. Brahim, and F. Segovia, 'Early diagnosis of Alzheimer's disease based on partial least squares, principal component analysis, and support vector machine using segmented MRI images," Neurocomputing, vol. 151, pp. 139–150, 2015.

[12] I. A. Illán et al., "Manuel Gómez-Rio, Carlos García Puntonet, and Alzheimer's Disease Neuroimaging Initiative," Information Sciences, vol. 181, no. 4, pp. 903–916, 2011.

[13] C. B. Granger et al., "Apixaban versus warfarin in patients with atrial fibrillation," New England Journal of Medicine, vol. 365, no. 11, pp. 981–992, 2011.

[14] ADNI. [Online]. Available: https://adni.loni.usc.edu. [Accessed: 15-Jan-2023].

[15] C. Li, J. C. Gore, and C. Davatzikos, "Multiplicative intrinsic component optimization (MICO) for MRI bias field estimation and tissue segmentation," Magnetic resonance imaging, vol. 32, pp. 913–923, 2014.

[16] J. Sled, A. Zijdenbos, and A. Evans, "A nonparametric method for automatic correction of intensity nonuniformity in MRI data," IEEE Trans Med Imaging, vol. 17, no. 1, pp. 87–97, 1998.

[17] N. Tustison, B. Avants, and P. Cook, "N4itk: improved n3 bias correction," IEEE Trans Med Imaging, vol. 29, no. 6, pp. 1310–1320, 2010.

[18] W. Wells, E. Grimson, R. Kikinis, and F. Jolesz, "Adaptive segmentation of MRI data," IEEE Trans Med Imaging, vol. 15, no. 4, pp. 429–442, 1996.

[19] C. R. Johnson and C. Hansen, Visualization Handbook. Academic Press, 2011.

[20] R. M. Haralick, K. Shanmugam, and I. Dinstein, "Textural features for image classification," Man, Cybern, vol. 3, pp. 610–621, 1973.

[21] S. Jafarpour, Z. Sedghi, and M. C. Amirani, "A robust brain MRI classification with GLCM features," International Journal of Computer Applications, vol. 37, no. 12, pp. 1–5, 2012.

[22] F. Ahmad and W. M. Da, "Classification of Alzheimer's disease stages: an approach using PCA-based algorithm," Journal of Alzheimer's Disease & Other Dementias®, vol. 33, no. 7, pp. 433–439, 2018.

[23] Y. Chen, L. Wang, and B. Ding, "Radiologically based automated segmentation of cardiac MRI using an improved U-Net neural algorithm,'' Journal of Radiation Research and Applied Sciences,2023.

[24] A. Y. Yew and M. Li, "Feature extraction of Alzheimer's disease classification based on principal component and random subspace discriminant analysis," J. Theor. Appl. Inf. Technol, 2021.

[25] D. N. S. Gonçalves and C. M. Gonçalves, "Analysis of the difference between the euclidean distance and the actual road distance in Brazil, ," Transportation Research Procedia, vol. 3, pp. 876–885, 2014.